Supplementary Materials and Methods (Metabolomics analysis)

Metabolite extraction and mass spectrometry analysis. 12 *Vldlr-/-* knock out and 12 wild type (WT) retinas were separately frozen at -80 ºC in 50µL PBS until used, at which point metabolites were extracted and proteins were precipitated by adding 600µL of cold acetone to the cell pellet. Samples were then vortexed-mixed for 30 sec and submerged for 1 min in liquid nitrogen followed by thawing (2-3 minutes) and sonication for 10 min at 50 ºC. This process was repeated three times followed by freezing at -20 ºC for 1h. The pellet was removed by centrifugation at 16,000 x g for 10 min and the supernatant was transferred to a clean tube. 400 µL of cold methanol/water/formic acid (86.5/12.5/1.0) was added to the pellet followed by vortex-mixing for 30 sec, sonication for 15 min at 50 ºC and freezing for 60 min at -20 ºC. The pellet was again removed by centrifugation at 16,000 x g for 10 min, and supernatant was pooled with the first extraction in the clean tube. Samples were dried in a SpeedVac to dryness. 100 µL of 95% ACN/water was added to the dried samples followed by vortex-mixing and sonication in a bath sonicator for 5 min. Samples were centrifuged at 16,000 x g and the supernatant was removed to a clean LC-MS vial. The samples were maintained at 4 ºC in the autosampler and analyzed by LC-MS.

Liquid chromatography-MS (LC-MS). 4 µL of processed retina sample were injected for each run. Reverse phase chromatography was performed using a 150 by 0.5mm (diameter) Zorbax C18 column with 5µm particles, at a flow rate of 20 µL/min. The LC system was an Agilent 1100 with a capillary pump. Buffer A was water with (+ ion mode) or without (- ion mode) 0.1% formic acid, and buffer B was acetonitrile with (+ ion mode) or without (- ion mode) 0.1% formic acid. For the endcapped C18 column, the column was equilibrated in 90% buffer A, and the samples were run with a gradient of 10%-98% over 60min. HILIC chromatography was performed using a 150 by 1.0mm (diameter) SeQuant ZIC®-HILIC column with 3.5µm particles, at a flow rate of

50 µL/min. The LC system was an Agilent 1100 with a capillary pump. Buffer A was water in 5mM ammonium acetate, and buffer B was 90% acetonitrile/10% water in 5mM ammonium acetate. The column was equilibrated in 90% B, and the samples were rung using a gradient of 90%-40% over 15min.

Mass Spectrometry. Data was collected in continuum mode from m/z 100 to 1000 using an Agilent ESI-TOF. The capillary voltage was 3500 V, with a nebulizer gas flow of 15 L/min. The instrument was calibrated immediately before use. The data files were converted from the instrument format (.wiff) to the common data format, using the PESciEX data translator. The XCMS program (Ref 1) was used to align and analyze the LC-MS data. To confirm the identification of significant ions, we used a quadrupole-TOF (Agilent 6520 Accurate-Mass Q-TOF). Masses for CID were targeted from a mass list and fragmented during the chromatography run.

Metabolite Database searching. Metabolites were identified by exact mass (m/z) using METLIN (http://metlin.scripps.edu/), Human Metabolome Project (http://redpoll.pharmacy.ualberta.ca/hmdb/HMDB/), Lipid Maps (http://www.lipidmaps.org/), Biological Magnetic Resonance Data Bank (http://www.bmrb.wisc.edu/) and KEGG ligand (http://www.genome.jp/kegg/ligand.html) databases.

Supplemental figure S1: Metabolomics analysis discovered multiple carnitine derivatives upregulated in *Vldlr-/-* retinas compared with WT retinas. (A) Metabolites from each isolated retina were extracted using acetone/methanol and applied to a capillary reversed phase (RP) or HILIC HPLC column interfaced to an ESI-TOF mass spectrometer in positive (+) and negative (-) ion mode to increase metabolite coverage (ref 1). Processing of raw data using the XCMS software resulted in time-aligned ion features, which were defined as a unique m/z at a unique retention time (ref 2). 3000-5000 features were found in the wild type (WT) and *VLDLR-/-* retina. Statistically significant differences were ranked using t-test statistical analyses in order to obtain quantitative information between WT and *Vldlr-/-* samples. (B) Identification of metabolites: accurate mass information by TOF (error $<$ 5ppm) was used for metabolite database searching. Test compounds were selected for each metabolite identified, and their HPLC retention times and collision-induced dissociation (CID) fragmentation patterns (Q-TOF MS) were compared with identified metabolite for conclusive confirmation of identification. Blue asterisks correspond to parent ions, exemplifying the identification of endogenous L-carnitine.

Selected references:

1. Smith, C. A., Want, E. J., O'Maille, G., Abagyan, R. & Siuzdak, G. XCMS: processing mass spectrometry data for metabolite profiling using nonlinear peak alignment, matching, and identification. Anal Chem 78, 779-87 (2006).

2. Nordstrom, A., Want, E., Northen, T., Lehtio, J. & Siuzdak, G. Multiple ionization mass spectrometry strategy used to reveal the complexity of metabolomics. Anal Chem 80, 421-9 (2008).

Supplemental Figure S1:

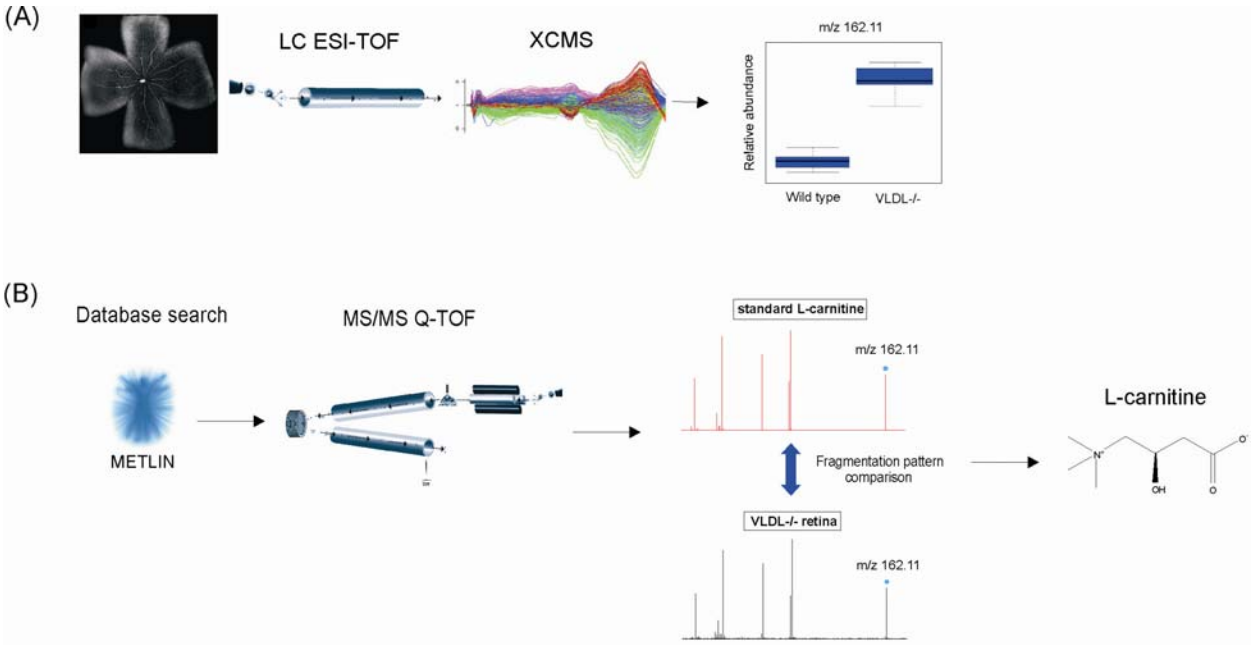

Name	Molecular Formula	m/z observed	p-value	Fold change	Up/down Regulation in *vldlr-/-*
L-carnitine	C7H15NO3	162.11	$5.45exp^{-6}$	2.58	↑
L-Acetylcarnitine	C9H17NO4	204.12	$1.03exp^{-10}$	3.00	↑
Isovalerylcarnitine	C12H23NO4	246.17	$2.55exp^{-6}$	2.28	↑
Isohydrosorbylcarnitine	C13H23NO4	258.16	$2.90exp^{-10}$	3.27	↑
Hexanoylcarnitine	C13H25NO4	260.18	$1.58exp^{-7}$	2.18	↑
Hydroxyoctanoylcarnitine	C15H29NO5	304.21	$6.66exp^{-7}$	3.39	↑
PC(18:1/0:0)	C26H52NO7P	522.35	$9.81exp^{-6}$	3.17	↓
PC(10:0/20:0)	C38H76NO8P	706.53	$7.42exp^{-8}$	1.93	↓
TG(22:6/22:6/22:6)	C69H98O6	1040.77	$1.89exp^{-5}$	2.22	↓
DG(22:6/22:6)	C47H68O5	730.54	$6.94exp^{-4}$	2.20	↓

Supplemental table 1: Large-scale microarray gene expression analysis was performed to test the expression of oxidative stress-related genes, particularly those involved in cellular defense mechanisms against oxidative stress. Overall, no differences in gene expression of these factors were found when comparing 3 week old *Vldlr-/-* mouse retinas to age-matched C57BL6/J wild-type retinas indicating that the observed increase in oxidative stress and subsequent neuronal degeneration is not directly related to the *Vldlr-/-* genetic defect, but rather is likely to be a consequence of the excessive intra- and subretinal NV that forms in the retinas of *Vldlr-/-* mice. Table 1 gives the raw data values of all the tested genes (obtained from the microarray analysis following the standard affymetrix protocol) that were found to be expressed in the retinas. Genes whose values differed >2-fold between Vldlr-/- and WT retinas are shown in red. Only one outlier, 9-cis-retinol dehydrogenase, demonstrated significantly different expression levels (>95%), although we have yet to determine a functional correlation between the expression levels of this gene and the *Vldlr-/-* retinal phenotype.

Gene Name	expression levels C57/Bl-6	vldlr-/-	fold change WT/vldlr	Genbank accession #	Gene product
Chaperones					
Hspa5	1680	1734	0.97	AI002387	BiP; chaperone
Grpel2	176	176	0.99	AF041060	co-chaperone mt-GrpE#2 precursor
Cct8	415	523	0.79	Z37164	haperonin containing TCP-1, theta subunit
Cctb	163	211	0.77	AB022156	chaperonin containing TCP-1, beta subunit
Cct7	1076	1216	0.88	Z31399	chaperonin containing TCP-1, beta subunit
Cctz-2	88	49	1.80	AB022086	chaperonin containing TCP-1, zeta-2 subunit
Cct5	1496	1821	0.82	Z31555	chaperonin containing TCP-1, epsilon subunit
heat shock proteins					
Hsf1	193	131	1.47	AF059275	heat shock transcription factor 1
Hsf2	17	15	1.11	X61754	heat shock transcription factor 2
Hsp60	1974	2234	0.88	X53584	heat shock protein 60; groEL gene
Hsp70-3	1196	934	1.28	M12571	heat shock protein, 68 kDa
Serpinh1	157	122	1.28	X60676	heat shock protein; HSP47 gene
Hsp86-1	8228	8536	0.96	J04633	heat shock protein, 86 kDa 1
Hsp84-1	4109	3529	1.16	M18186	heat shock protein, 84 kDa 1
Dnajb1	555	487	1.14	AB028272	heat shock protein 40
Hsc70-8	2347	2699	0.87	X54401	heat shock protein, 70 kDa - 8
Hsp105	807	790	1.02	L40406	heat shock protein, 105 kDa
Hsp70-2	25	25	0.97	M20567	heat shock protein, 70 kDa - 2
crystallins					
Crybb2	25	33	0.78	M60559	beta-B2 crystallin
Cryaa	147	111	1.33	J00376	alpha-crystallin; crystallin
murine gamma E-crystallin	217	150	1.45	X57855	gamma E-crystallin
Cryga	9	9	1.02	K02587	gamma A crystallin
CrygD	126	84	1.50	AI224342	gamma-D-crystallin
Crym	312	517	0.60	AF039391	mu-crystallin
alphaA-CRYBP1	185	239	0.78	L36829	alphaA-crystallin-binding protein I
Crygs	127	98	1.30	AF032995	gammaS-crystallin
CrygB	25	14	1.70	Z22573	gamma-B-crystallin
CrygF	271	115	2.36	AI224343	gamma-F-crystallin
Cryz	139	191	0.73	D78646	zeta-crystallin/quinone reductase
peroxidases					
Mpo	43	26	1.69	X15378	precursor myeloperoxidase
Gpx3	152	193	0.79	U13705	plasma glutathione peroxidase precursor
GSHPx	316	299	1.06	X03920	glutathione peroxidase
Gpx4	928	924	1.00	D87896	phospholipid hydroperoxide glutathione peroxidase
Tpo	26	42	0.62	X60703	peroxidase
Prdx2	407	491	0.83	U20611	peroxidase
Gpx2-ps1	148	129	1.15	X91864	selenocysteine; glutathione peroxidase-GI
reductases					
Rrm1	108	126	0.86	K02927	ribonucleotide reductase M1
Th	99	123	0.80	M69200	tyrosine hydroxylase; oxygen oxidoreductase
NG28	2731	2902	0.94	AF110520	NADH oxidoreductase
Mod1	862	720	1.20	J02652	malate oxidoreductase
NG28	229	224	1.02	AF110520	NADH oxidoreductase
NG28	304	216	1.41	AF110520	NADH oxidoreductase
Rsdr1-pending	338	231	1.47	X95281	retinal short-chain dehydrogenase/reductase
Akr1e1	109	149	0.73	U68535	aldo-keto reductase
Lorsdh	28	40	0.69	AI224761	lysine ketoglutarate reductase
Hmgcr	390	400	0.97	M62766	HMG-CoA reductase
Txnrd2	73	68	1.08	AB027566	thioredoxin reductase 2
Fdxr	116	93	1.25	D49920	Ferredoxin-NADP Reductase precursor
Cbr2	44	20	2.14	D26123	carbonyl reductase
Scd1	108	248	0.44	M21285	cytochrome b-5 reductase
Sqle	762	917	0.83	D42048	squalene epoxidase
Nqo1	43	43	1.00	U12961	NAD(P)H:menadione oxidoreductase
NG28	2269	2825	0.80	AF110520	NADH oxidoreductase
Cbr1	243	253	0.96	U31966	carbonyl reductase
NG28	184	227	0.81	AF110520	NADH oxidoreductase
NG28	87	107	0.81	AF110520	NADH oxidoreductase
Dhcr7	162	185	0.87	AF057368	delta7-sterol reductase
Por	382	416	0.92	D17571	NADPH-cytochrome P450 oxidoreductase
Txnrd1	277	284	0.98	AB027565	thioredoxin reductase 1

Gene Name	expression levels C57/Bl-6	vldlr-/-	fold change WT/vldlr	Genbank accession #	Gene product
dehydrogenases					
Aldh1a1	617	533	1.16	M74570	aldehyde dehydrogenase II
Impdh2	447	455	0.98	M33934	inosine 5'-phosphate dehydrogenase 2
Rdh7	57	41	1.40	AF056194	short-chain dehydrogenase CRAD2
Nqo1	25	22	1.11	M36660	NAD(P)H dehydrogenase, quinone 1
Gapd	8484	9091	0.93	M32599	glyceraldehyde-3-phosphate dehydrogenase
G6pd-2	432	486	0.89	Z84471	glucose-6-phosphate dehydrogenase
Rdh5	301	59	5.11	AF033195	9-cis-retinol dehydrogenase
Bckdk	478	454	1.05	AF043070	branched chain alpha ketoacid dehydrogenase kinase
Ldh2	548	662	0.83	X51905	lactate dehydrogenase 2, B chain
Ugdh	786	1170	0.67	AF061017	UDP-glucose dehydrogenase
Ke 6	52	52	1.00	U34072	steroid dehydrogenase
Hsd3b1	21	23	0.88	M58567	3-beta-hydroxysteroid dehydrogenase
Acads	41	38	1.06	L11163	short chain acyl-CoA dehydrogenase
Dhodh	154	234	0.66	AF029667	dihydroorotate dehydrogenase
Gcdh	758	613	1.24	U18992	glutaryl-CoA dehydrogenase precursor
Idh1	315	650	0.48	AF020039	NADP-dependent isocitrate dehydrogenase
Acadm	939	1262	0.74	U07159	medium-chain acyl-CoA dehydrogenase
Glud	312	306	1.02	X57024	glutamate dehydrogenase (NAD(P)+)
Hsd3b4	32	21	1.51	L16919	3-beta-hydroxysteroid dehydrogenase
Idh3g	701	936	0.75	U68564	NAD(H)-specific isocitrate dehydrogenase
Hpgd	81	96	0.85	U44389	NAD(+)-dependent 15-hydroxyprostaglandin dehydrogenase
MDH	3459	3343	1.03	X07295	malate dehydrogenase
Hsd17b12	938	1323	0.71	AF064635	putative steroid dehydrogenase
Aldh1a7	48	54	0.90	U96401	aldehyde dehydrogenase Ahd-2-like
G6pdx	359	467	0.77	Z11911	glucose-6-phosphate dehydrogenase
Acadl	45	36	1.25	U21489	long-chain acyl-CoA dehydrogenase
Hadhsc	171	188	0.91	D29639	3-hydroxyacyl CoA dehydrogenase
Aldh2	244	213	1.14	U07235	aldehyde dehydrogenase
Ldh1	10183	8568	1.19	M17516	lactate dehydrogenase 1, A chain
Dld	815	952	0.86	U73445	dihydrolipoamide dehydrogenase
Mor2	190	125	1.52	M29462	malate dehydrogenase
Hsd17b4	228	354	0.65	X89998	17beta-hydroxysteroid dehydrogenase IV
Pdha1	1034	1272	0.81	M76727	pyruvate dehydrogenase
Ndufa1	7	9	0.84	Y07708	NADH dehydrogenase
Impdh1	2426	1696	1.43	U00978	type I inosine monophosphate dehydrogenase
Adh5	891	1092	0.82	M84147	alcohol dehydrogenase-B2
Gdm1	99	115	0.86	D50430	glycerol-3-phosphate dehydrogenase
aldh3	35	59	0.59	AF033034	aldehyde dehydrogenase 3
Aldh3a2	260	315	0.83	U14390	aldehyde deydrogenase
redoxins					
Prxll-2	2618	2950	0.89	AF032714	type II peroxiredoxin protein 2
Prdx5-rs3	435	595	0.73	AF093853	1-Cys peroxiredoxin protein 2
Prdx5	663	936	0.71	AF093857	1-Cys peroxiredoxin protein
Txnl	190	198	0.96	AF052660	thioredoxin-related protein
Txn1	1083	1367	0.79	X77585	thioredoxin-1
Glrx1	270	272	1.00	AB013137	glutaredoxin
red-1	29	31	0.92	X92750	nucleoredoxin
Prdx1	1044	1482	0.70	AB023564	type I peroxiredoxin
Txn2	977	725	1.35	U85089	thioredoxin-2
Unclassified genes					
Pdcd8	324	452	0.72	AF100927	apoptosis-inducing factor AIF
MnSOD	149	221	0.67	L35528	manganese superoxide dismutase
Fth	3765	3782	1.00	X52561	ferrerin H subunit
Sod1	947	1000	0.95	M35725	Cu-Zn-superoxide dismutase
Sqstm1	975	1014	0.96	U40930	oxidative stress-induced protein
Ftl1; Ftl-1	2271	2232	1.02	L39879	ferritin L-subunit